THE ASTROPHYSICAL JOURNAL, 212:149–158, 1977 February 15

PRODUCTION OF ^{14}C AND NEUTRONS IN RED GIANTS

JOHN J. COWAN AND WILLIAM K. ROSE
Astronomy Program, University of Maryland, College Park
Received 1976 June 28

ABSTRACT

We have examined the effects of mixing various amounts of hydrogen-rich material into the intershell convective region of red giants undergoing helium shell flashes. We find that significant amounts of ^{14}C can be produced via the $^{14}N(n, p)^{14}C$ reaction. If substantial portions of this intershell region are mixed out into the envelopes of red giants, then ^{14}C may be detectable in evolved stars.

We find a neutron number density in the intershell region of $\sim 10^{15}$–10^{17} cm^{-3} and a flux of $\sim 10^{23}$–10^{25} cm^{-2} s^{-1}. This neutron flux is many orders of magnitude above the flux required for the classical *s*-process, and thus an intermediate neutron process (*i*-process) may operate in evolved red giants. The neutrons are principally produced by the $^{13}C(\alpha, n)^{16}O$ reaction.

In all cases studied we find substantial enhancements of ^{17}O. These mixing models offer a plausible explanation of the observations of enhanced ^{17}O in the carbon star IRC 10216. For certain physical conditions we find significant enhancements of ^{15}N in the intershell region.

Subject headings: nucleosynthesis — stars: abundances — stars: interiors — stars: late-type

I. INTRODUCTION

There is a great deal of observational evidence that nucleosynthesis is taking place in the interiors of red giants. S stars and luminous carbon stars almost certainly originate from nucleosynthesis during helium shell flashes. The principal goal of this paper is to predict the relative production of the isotopes of light elements and neutron fluxes that may be produced as a result of helium shell flashes.

Numerous stellar model calculations have indicated that helium shell flashes occur in red giants as these double-shell-burning stars ascend the red giant branch for the second time (i.e., after helium core burning). In general the violence of these shell flashes increases as these stars evolve and become more luminous. An extensive intershell convective zone is produced as a result of these helium shell flashes. Although Schwarzschild and Härm (1967) found that this convective zone penetrated into the hydrogen-rich layers, other calculations (e.g., Rose and Smith 1970, 1972; Sweigart 1974; Gingold 1974) showed that for low-mass stars the intershell convective zone closely approaches but does not penetrate the hydrogen shell. More recent calculations (Christy-Sackmann 1976) indicate that the intershell convective zone of a 6 $M_\odot$ star approaches to within 0.5 density scale heights of the hydrogen shell. Although most of the previously published calculations do not predict that the intershell convective zone will penetrate the hydrogen-rich layers above it, it is plausible in view of the approximate nature of stellar model calculations that such penetration does arise as a result of physical processes that have not been included in the calculations. Sanders (1967) has shown that mixing under physical conditions such as we have described can lead to the production of significant neutron fluxes in the intershell convective zone.

In the calculations that are described below we will assume that mixing between the intershell region and the hydrogen-rich envelope occurs as a result of physical mechanisms not included in stellar model calculations. Overshooting of convective elements from the top of the intershell convective layer is a plausible mechanism for mixing beyond the computed convective boundaries. The problem of overshooting has been studied by Roxburgh (1965), Shaviv and Salpeter (1973), Castellani, Giannone, and Renzini (1971), Maeder (1975), and Cogan (1975).

Instabilities related to differential rotation, which must occur as envelope material is processed through the hydrogen shell, represent another class of plausible mixing mechanisms. Conservation of angular momentum implies that the rotational velocity of matter should increase by many orders of magnitude as the envelope material moves from the base of the convective envelope through the hydrogen-burning shell. Since it is plausible to assume that the intershell region is made to corotate during a helium shell flash, regions with steep gradients in their angular velocity are likely to be produced (Levy and Rose 1974). These steep gradients in angular velocity can lead to an instability of the type discussed by Goldreich and Schubert (1967). The Goldreich and Schubert instability may lead to the turbulent diffusion of angular momentum whenever the angular momentum per unit mass decreases outward. Mixing caused by this instability is likely to proceed on a thermal time scale (Kippenhahn 1969). Since this time scale is comparable to the duration of the maximum extent of the intershell convective zone, there is likely to be sufficient time for

the transport of angular momentum unless the relevant transport time scale is much longer (James and Kahn 1970). In this case mixing caused by this process would be negligible.

Shear turbulence in the presence of a gravitational field is a similar mixing mechanism. In this case the relevant parameter for stability is the Richardson number for compressible fluids. For sufficiently small values of the Richardson number, turbulent redistribution of angular momentum occurs in a dynamical time scale (Rood and Ulrich 1974). It is quite plausible that such small values of the Richardson number can be attained during a helium shell flash and consequently the turbulent redistribution of angular momentum should proceed rapidly over the unstable layer.

II. CALCULATIONS

We consider a red giant that is undergoing helium shell flashes. The mass interior to the helium-burning shell is taken to be 1 $M_\odot$. We assume that during a helium shell flash a convection zone extends all the way from the helium-burning shell to the hydrogen-burning shell. In carrying out this calculation we assumed a temperature $T = 3 \times 10^8$ K, density $\rho = 2 \times 10^3$ g cm^{-3}, and radius $R = 10^9$ cm at the boundary of the core. This boundary is taken to be just above the helium-burning shell. A knowledge of the physical variables at the core boundary and the further assumption of adiabatic convection allow us to determine the values of the physical variables in the intershell region by means of standard numerical integration.

Following Iben (1975) we assume that the hydrogen-burning shell is reached when $T \sim 75 \times 10^6$ K. The initial composition of the intershell region (assumed uniform) was $^{12}C = 0.2$, $^4He = 0.78$, and $^{16}O = 0.02$ by mass. Those values are in rough agreement with those of Christy-Sackmann and Paczynski (1975). We varied the intershell composition so that ^{12}C was more abundant than ^4He and found the same qualitative results as we found for the above composition. We calculated how much matter is included in one pressure scale height above the hydrogen shell. We then mixed in fractions of a scale height of matter (10^{-4}–10^{-2}), assuming a solar composition of hydrogen and helium ($X = 0.75$ and $Y = 0.23$). We made the assumption that the remaining 2% of all the matter initially mixed into the intershell region was ^{14}N that had been produced by CNO burning in the hydrogen shell.

The upper limit of 10^{-2} scale heights was chosen because this choice corresponded to $+2.5 \times 10^{-6}\ M_\odot$ of hydrogen above the hydrogen shell. Since 1 $M_\odot$ of hydrogen is capable of releasing $\sim 10^{52}$ ergs during nuclear burning, 10^{-2} scale heights corresponds to $\sim 10^{46}$ ergs. Energies less than this will not produce violent hydrogen shell flashes, such as those that occur in novae (Rose 1968; Starrfield *et al.* 1972). Such a violent event would significantly change the run of temperature and density in the intershell region, and consequently we did not mix larger amounts of hydrogen from the envelope into the intershell region.

Our upper limit of 10^{-2} scale heights ($2.5 \times 10^{-6}\ M_\odot$) is also an appropriate choice as this value corresponds to the maximum amount of mixed hydrogen-rich matter that was included in the studies of Sweigart (1974) who was examining the response of the flash convective zone to different amounts of hydrogen mixing in a 0.7 $M_\odot$ Population II star. This value of $\sim 2 \times 10^{-6}\ M_\odot$ was approximately 10 times the maximum amount of hydrogen that was found by Schwarzschild and Härm (1967) to be mixed into the intershell region during one helium shell flash cycle in a 1 $M_\odot$ star.

Assuming that the hydrogen shell is located at about $T = 75$–80×10^6 K, we find that the helium- and hydrogen-burning shells are separated by approximately 1.2×10^9 cm. The pressure scale height H_p is given by

$$H_p^{-1} = \frac{1}{P}\left|\frac{dP}{dr}\right|; \tag{1}$$

and for our case $H_p \approx 2 \times 10^8$ cm.

We assume that this matter of solar composition (with all the heavy elements in the form of ^{14}N) is convected from the hydrogen shell down to the helium shell in a diffusion time τ_d. Since this intershell region extends over several pressure scale heights (i.e., ~ 6), we use the diffusion approximation to estimate the diffusion time. If such an approximation is used, the time scale for matter to traverse a thickness ΔR is

$$\tau_d \approx \left(\frac{\Delta R}{v_c}\right)\left(\frac{\Delta R}{\lambda}\right), \tag{2}$$

where λ is the mixing length and v_c is the convective velocity in the intershell region given by (Levy and Rose 1974)

$$v_c \approx 10^3 (L_{\rm He}/L_\odot)^{1/3}\ \text{cm s}^{-1}. \tag{3}$$

For a typical peak luminosity of $L_{\rm He} \approx 10^6\ L_\odot$, $v_c \approx 1$ km s^{-1}. If we let $\lambda = H_p$, then $\tau_d \approx 6\tau_c$ where τ_c is the convective time scale given by

$$\tau_c = \Delta R / v_c. \tag{4}$$

For $\Delta R = 1.2 \times 10^9$ cm and $v_c = 1$ km s^{-1}, equation (2) gives $\tau_d \sim 7.2 \times 10^4$ s.

As this matter moves downward, it is mixed into the intershell region and burned. We divided the intershell region into 50 equal mass zones (each zone contains $1.4 \times 10^{-4}\ M_\odot$). The average time for matter to be convected through a zone is approximately 10^3 s.

The lifetime $\tau_b(a)$ of some species a against reactions with some species b is given by (Clayton 1968)

$$\tau_b(a) = (N_b \langle \sigma v \rangle_{ab})^{-1}, \tag{5}$$

where $\langle \sigma v \rangle_{ab}$ is the reaction rate between particles; and the number density of species b is

$$N_b = \rho N_A X_b / A_b, \tag{6}$$

where ρ is the mass density, N_A is Avogadro's number,

X_b the mass fraction of b, and A_b the atomic weight of species b. The quantity $N_A\langle\sigma v\rangle_{ab}$ is conveniently listed in Fowler, Caughlan, and Zimmerman 1975 (FCZ II). In the intershell region the lifetimes of the nuclear species against hydrogen and helium burning given by equations (2) and (3) are in general much longer than 10^3 s (i.e., $\tau > 10^4$ s). The exception to the above statement is the reaction $^{15}N(p, \alpha)^{12}C$, where τ is comparable to or slightly less than 10^3 s for several of the densities and temperatures encountered. This reaction rate, which is very uncertain, does not seem to greatly affect abundance changes in our case. (We checked this by running several cases with more [i.e., smaller] zones.) Since the lifetimes of the nuclear species against hydrogen and helium burning are in general longer than the time for convection through a zone ($\tau \sim 10^3$ s), we must first mix the matter coming from a higher zone into the new zone before initiating nuclear burning. After the matter had been mixed into a zone, we turned on all of the nuclear reactions for a time equal to the time it would take matter to be convected through a zone. The midpoint temperature and density of each zone was used in carrying out the calculations. Initially all of the zones contain only ^{4}He, ^{12}C, and ^{16}O, so the other elements become diluted in concentration due to the mixing (although they can build up due to nuclear reactions). After nuclear burning has continued for the required time scale, we then mix the matter from this burning zone to the next unburned zone and recompute the mass fractions and continue burning. This process is repeated until the helium-burning shell is reached at $T = 3 \times 10^8$ K.

We have checked that our basic results do not depend appreciably on whether matter is mixed at the convective velocity or at a slower rate that is consistent with the diffusion approximation. Since these two approximations should bracket physically plausible mixing velocities, we believe that our basic results are independent of uncertainties in the dynamics of turbulent mixing.

The network of nuclear reactions that we used contains 21 species (including neutrons and protons) and is similar to the network used in Cowan and Rose (1975, hereafter Paper I). We have added the important reaction $^{22}Ne(\alpha, n)^{25}Mg$ and several (n, γ) reactions not included in Paper I. The nuclear reaction rates with the appropriate references are listed in Table 1, and a schematic representation of all the reactions except $^{22}Ne(\alpha, n)^{25}Mg$ is shown in Figure 1. Some of these reaction rates from FCZ II have the factor 0 to 1 front of several terms (we referred to these 0 and 1 factors as θ in Paper I). We found that our results were virtually independent of the value of these θ parameters.

The initial time step in each mass zone was very small (10^{-10} s), and the abundances of all elements with mass

TABLE 1

NUCLEAR REACTION RATES

Strong Interactions	
$^4He(2\alpha, \gamma)^{12}C$	(FCZ II)
$^{12}C(p, \gamma)^{13}N$	(FCZ II)
$^{12}C(n, \gamma)^{13}C$	(FCZ I)
$^{12}C(\alpha, \gamma)^{16}O$	(FCZ II)
$^{13}N(p, \gamma)^{14}O$	(FCZ II)
$^{13}N(n, p)^{13}C$	(FCZ II)
$^{13}C(p, \gamma)^{14}N$	(FCZ II)
$^{13}C(n, \gamma)^{14}C$	(FCZ I)
$^{13}C(\alpha, n)^{16}O$	(FCZ II)
$^{14}C(p, \gamma)^{15}N$	(FCZ II)
$^{14}C(\alpha, \gamma)^{18}O$	(W)
$^{14}N(p, \gamma)^{15}O$	(FCZ II)
$^{14}N(n, \gamma)^{15}N$	(FCZ I)
$^{14}N(n, p)^{14}C$	(FCZ II)
$^{14}N(\alpha, \gamma)^{18}F$	(FCZ II)
$^{15}N(p, \gamma)^{16}O$	(FCZ II)
$^{15}N(p, \alpha)^{12}C$	(FCZ II)
$^{15}N(\alpha, \gamma)^{19}F$	(FCZ II)
$^{16}O(p, \gamma)^{17}F$	(FCZ II)
$^{16}O(n, \gamma)^{17}O$	(FCZ I)
$^{16}O(\alpha, \gamma)^{20}Ne$	(FCZ II)
$^{17}O(p, \gamma)^{18}F$	(FCZ II)
$^{17}O(p, \alpha)^{14}N$	(FCZ II)
$^{17}O(\alpha, n)^{20}Ne$	(FCZ II)
$^{18}O(p, \gamma)^{19}F$	(FCZ II)
$^{18}O(p, \alpha)^{15}N$	(FCZ II)
$^{18}O(\alpha, \gamma)^{22}Ne$	(FCZ II)
$^{18}O(\alpha, n)^{21}Ne$	(FCZ II)
$^{19}F(p, \gamma)^{20}Ne$	(FCZ II)
$^{19}F(p, \alpha)^{16}O$	(FCZ II)
$^{22}Ne(\alpha, n)^{25}Mg$	(FCZ II)
Weak Interactions: λ in s^{-1}	
$^{13}N(\beta^+\nu)^{13}C$	1.16×10^{-3}
$^{14}O(\beta^+\nu)^{14}N$	9.76×10^{-3}
$^{15}O(\beta^+\nu)^{15}N$	5.68×10^{-3}
$^{17}F(\beta^+\nu)^{17}O$	1.05×10^{-2}
$^{18}F(\beta^+\nu)^{18}O$	1.05×10^{-4}

NOTE.—FCZ I = Fowler, Caughlan and Zimmerman 1967; FCZ II = Fowler, Caughlan and Zimmerman 1975; W = Wagoner 1969.

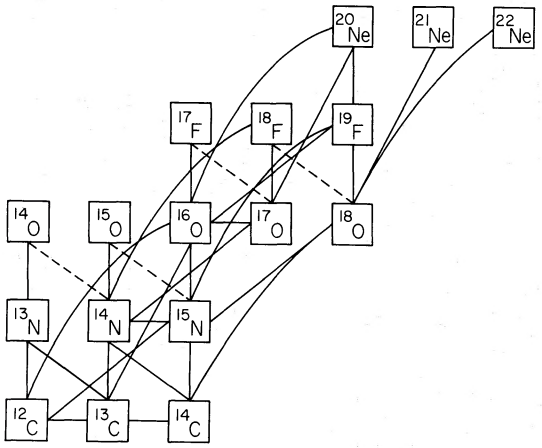

FIG. 1.—The network of nuclear reactions that we used in our calculations. [The $^{22}Ne(\alpha, n)^{25}Mg$ reaction is not shown in the figure, although it was included in the network.] The vertical lines represent (p, γ) reactions, and the horizontal lines represent (n, γ) reactions, between nuclei. The lines of approximately 60° angle (from the horizontal) are (α, n) reactions, and the lines of 40° angle are (α, p) and (p, α) reactions. The curved lines are (α, γ) reactions. The solid lines at 135° (from the horizontal) represent (n, p) reactions. The dashed lines represent positron (β^+) decays of unstable nuclei.

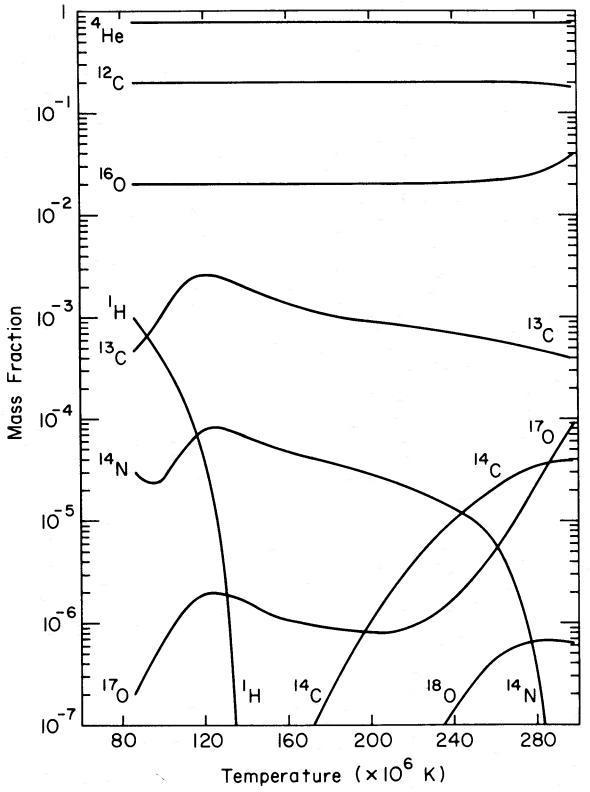

FIG. 2.—The variations in the isotopic mass fraction that occur in the intershell convective region when $10^{-3}H_p$ of hydrogen-rich matter ($\approx 3 \times 10^{-7}\ M_\odot$) is mixed into the intershell region. The initial composition of the intershell region is ^{4}He = 0.78, ^{12}C = 0.2, and ^{16}O = 0.02. The temperature scale represents the run of temperature from the hydrogen shell at $T \sim 80 \times 10^6$ K to the helium shell at $T \sim 300 \times 10^6$ K. The temperature scale is analogous to a time scale since matter is convected downward (i.e., to higher temperatures) at constant velocity.

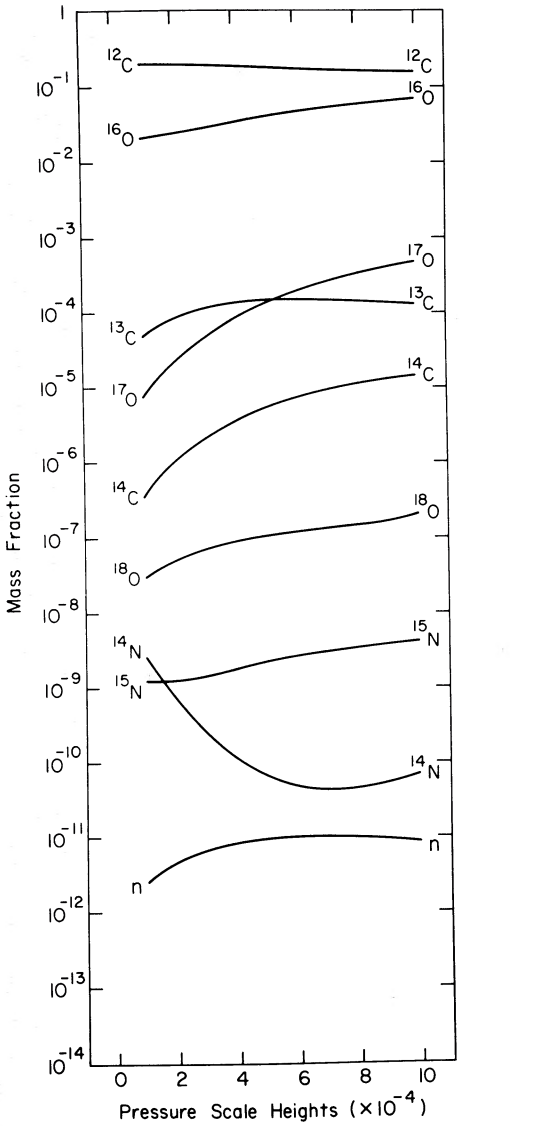

FIG. 3.—This illustrates the case where $10^{-3}H_p$ of matter is continuously mixed into the intershell region in 10 separate injections of $10^{-4}H_p$. The final abundance of every isotope is plotted after each $10^{-4}H_p$ has been completely mixed into the intershell region. The ^{4}He mass fraction was essentially constant throughout the mixing time-period, and thus it was not plotted in the figure.

fraction larger than 10^{-10} changed by less than 10% during each subsequent time step. We used the same fully implicit method in solving the various differential equations as was outlined in Paper I. As a test of the accuracy of our solutions we varied our choice of initial time step and found no difference in our results.

III. DISCUSSION AND RESULTS

Our results are displayed in Figures 2–5. In Figure 2 and Figure 4 the scales are mass fractions of the isotopes versus temperature. These plots indicate the variation in the isotopic abundances in the intershell convection zone as matter is convected downward from the hydrogen shell to the helium shell. The temperature scale represents the run of temperature from the hydrogen shell at $T \approx 80 \times 10^6$ K to the helium shell at $T \approx 300 \times 10^6$ K. The temperature scale is also analogous to a time scale since we are following matter as it is mixed downward (i.e., to higher temperatures) at a constant velocity of $\frac{1}{6}v_c$. When the intershell region has been completely mixed, the isotopic abundances throughout the convective region will be essentially the same as they are at the edge of the helium shell (i.e., the right-hand side of Figs. 2 and 5). We showed previously that the time for matter to be convected from the hydrogen shell to the helium shell, τ_d, was approximately 7.2×10^4 s. Since the intershell convection zone in an intermediate-mass star ($M = 6\ M_\odot$) will exist for approximately 100 years after the peak of the helium shell flash (Christy-Sackmann and Paczynski 1975), the intershell region will be completely mixed long before the convective zone disappears.

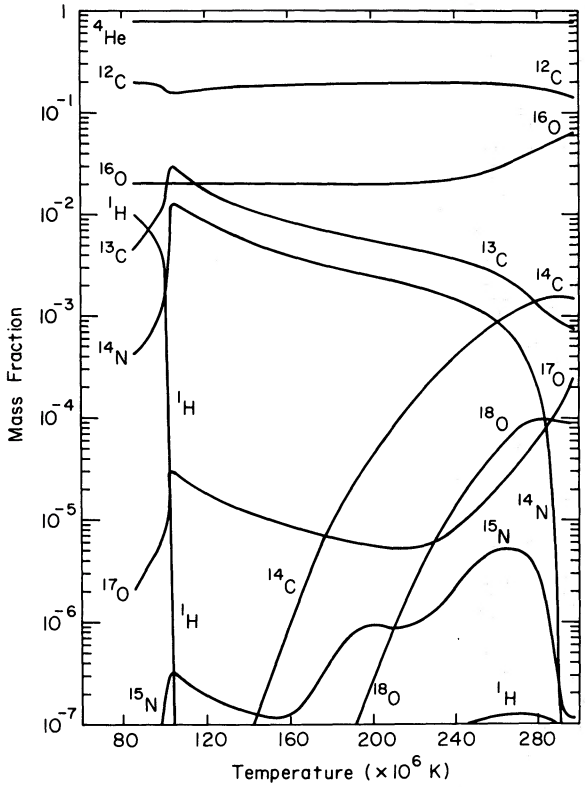

FIG. 4.—The variations in the isotopic mass fractions that occur in the intershell convective region when $10^{-2}H_p$ ($\approx 2.7 \times 10^{-6}\ M_\odot$) of hydrogen-rich matter is mixed into the intershell region. The matter is first convected from the hydrogen shell down to $T \approx 10^8$ K. At this point the hydrogen-rich matter was burned in a thin shell that split the convective zone. After the luminosity due to hydrogen burning dropped to less than $10^3\ L_\odot$ (in 1.7×10^5 s) the matter was then diffused down to the helium shell in the same manner that was used for the diffusion of $10^{-3}H_p$.

a) Rapid Mixing of 10^{-3} *Pressure Scale Heights*

Figure 2 illustrates the case where 10^{-3} of a pressure scale height of matter is mixed into the intershell region. In our case $10^{-3}H_p \approx 3 \times 10^{-7}\ M_\odot$. This is approximately the mass of hydrogen that Schwarzschild and Härm (1967) found was mixed into the intershell region of a 1 $M_\odot$ star during one helium shell flash cycle ($\sim 10^7$ s). The intershell region is initially composed of ^{4}He = 0.78, ^{12}C = 0.2, and ^{16}O = 0.02 by mass, and the matter mixed in is essentially solar ($X = 0.75$ and $Y = 0.23$), with the remaining 2% of heavy elements in the form of ^{14}N. As shown in Figure 2, hydrogen is rapidly burned while the CNO isotopes ^{13}C, ^{14}N, and ^{17}O are quickly enhanced. This buildup of isotopes is typical of CNO cycle hydrogen burning. The initial drop in the ^{14}N abundance is due to the dilution of ^{14}N as it is mixed downward. The subsequent buildup in the ^{14}N mass fraction is again typical of CNO burning and results from the slow reaction rate (i.e., large τ) for the ^{14}N$(p, \gamma)^{15}$O reaction.

It should be noted that at various times during this high-temperature burning some radioactive isotopes

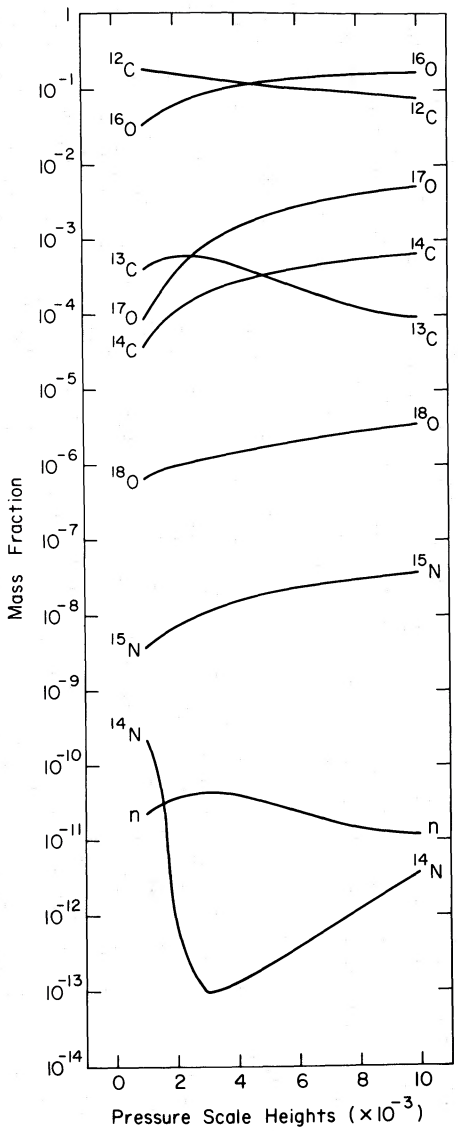

FIG. 5.—This illustrates the case where $10^{-2}H_p$ of matter is continuously mixed into the intershell region in 10 separate mixings of $10^{-3}H_p$. The final abundance of every isotope is plotted after each $10^{-3}H_p$ has been completely mixed into the intershell region. The ^{4}He mass fraction was essentially constant throughout the mixing time-period, and thus it was not plotted in the figure.

are more abundant than some stable isotopes. The abundances of the isotopes (except ^{14}C) plotted in Figures 2–5 are obtained by letting the radioactive nuclei β^+-decay to the stable isotopes. These β^+ decays take place on time scales of seconds. The radioactive isotope ^{14}C, which β-decays to ^{14}N, has a half-life of 5730 years and was plotted separately.

At temperatures above 240×10^6 K the isotopic abundances begin to change rapidly as illustrated in Figure 2. At these high temperatures the ^{13}C$(\alpha, n)^{16}$O reaction becomes the most important neutron producing reaction. This reaction is responsible for depressing

the ^{13}C abundance and building up the ^{16}O abundance. The neutrons that are produced are then captured by the neutron poison ^{14}N in the reaction $^{14}N(n, p)^{14}C$. This accounts for the dramatic rise in the ^{14}C abundance. By the time the helium shell is reached, the ^{14}N abundance has begun to drop drastically so it no longer can act as a neutron sink. At this point $^{13}N(n, p)^{13}C$ becomes the most important neutron poison. The importance of this reaction in capturing neutrons has been pointed out by Despain (1975). Shortly after the ^{14}N abundance drops, the ^{13}N abundance (not shown on the graphs) begins to drop and $^{12}C(n, \gamma)^{13}C$ becomes an important neutron-capture reaction. Since the ^{12}C abundance will never drop to very low values (as it is being produced in the helium shell) in the intershell region, the $^{12}C(n, \gamma)^{13}C$ reaction remains an important neutron sink even at very high temperatures.

Figure 2 also illustrates an enhancement of ^{17}O in the high-temperature region near the helium burning shell. Observations of enhanced ^{17}O have been reported for the carbon star IRC 10216 (Rank, Geballe, and Wolman 1974), and we feel that this is strong evidence that ^{17}O is being synthesized in red giants. We have already noted in Paper I that we expect a buildup of ^{17}O in high-temperature burning regions typical of evolved red giants. It has also been pointed out that ^{17}O may be enhanced during low-temperature (i.e., $T < 10^8$ K) CNO cycle hydrogen burning (Rolfs and Rodney 1974; Dearborn and Schramm 1974). In Paper I, however, we only treated high-temperature static burning. In the present case, where we are simulating mixing in red giants, we still find an enhancement of ^{17}O. Once the ^{17}O is produced in the intershell region, it can then be mixed out into the convective envelope during the phase following a shell flash when the convective envelope penetrates the intershell region (Iben 1975). Eventually this processed material can be expelled in a shell surrounding the star. We feel that this is a plausible explanation of the observations of enhanced ^{17}O IRC 10216.

The buildup of ^{17}O in the interior as shown in Figure 2 results mainly from the $^{16}O(p, \gamma)^{17}F(\beta^+\nu)^{17}O$ reaction. The $^{16}O(n, \gamma)^{17}O$ reaction is not as important in this case. The uncertainties in the nuclear reaction rates (the θ parameters) seem to affect the ^{17}O abundance more than any other isotope. We first noted this in Paper I. In Figure 2 we have set all the θ's (0 to 1 terms) equal to zero. By setting all the θ parameters equal to one, the ^{17}O abundance will be down by approximately 5% from the values shown in Figure 2. All of the other isotopes are essentially unchanged no matter what values are chosen for these uncertain nuclear reaction rates. The ^{18}O abundance shown in Figure 2 is due to the $^{14}N(\alpha, \gamma)^{18}F(\beta^+\nu)^{18}O$ and $^{17}O(p, \gamma)^{18}F(\beta^+\nu)^{18}O$ reactions. The $^{14}C(\alpha, \gamma)^{18}O$ reaction rate listed by Wagoner (1969) does not contribute greatly to ^{18}O production in our case.

b) *Continuous Mixing of* 10^{-3} *Pressure Scale Heights*

Even though the mass of the hydrogen mixed into the intershell region illustrated in Figure 2 was the same amount used in the stellar model calculations of Sweigart (1974), our rate of hydrogen mixing was faster than he assumed. To determine what differences this mixing rate would have on the isotopic abundances, we have attempted to simulate continuous mixing of hydrogen into the intershell region. This kind of mixing might occur as a result of convective overshooting. We first mixed into the intershell region

$$10^{-4}H_p(\approx 3 \times 10^{-8}\ M_\odot)$$

of essentially solar material from the envelope. We then let this matter become fully mixed throughout the intershell region (in $\sim 10^5$ s) and then mixed into the intershell region another $10^{-4}H_p$ of matter and allowed this matter to become fully mixed in the convective region. We repeated this process until we had mixed a total of 10^{-3} scale heights of matter into the intershell region. The results of this continuous mixing are shown in Figure 3, where we have plotted the final abundance of each isotope after each $10^{-4}H_p$ has been mixed into the intershell region. We have included in Figure 3 some of the less abundant isotopes (^{14}N, ^{15}N, and n) not shown in Figure 2. In general the isotopic abundances obtained after mixing in $10 \times 10^{-4}H_p$ continuously are roughly the same as in the case where we mix in $10^{-3}H_p$ illustrated in Figure 2.

The drop in ^{13}C and buildup of ^{16}O due to the $^{13}C(\alpha, n)^{16}O$ reaction (that was noted in Fig. 2) is again evident in Figure 3. The enhancement of ^{14}C due to the $^{14}N(n, p)^{14}C$ reaction is also again evident in the case of continuous mixing. The ^{17}O abundance is also increasing as in Figure 2, and the ^{17}O mass fraction is again much larger than the ^{18}O mass fraction. The ^{15}N abundance is quite low in Figure 3, although it is increasing gradually. The neutron abundance varies gradually reaching a peak mass fraction of 10^{-11}.

As shown in Figure 3, all except one of the isotopic abundances obtained by 10 separate mixings of $10^{-4}H_p$ are within a factor of approximately 3 of the isotopic abundances obtained by mixing $10^{-3}H_p$ into the intershell region. The exception is ^{17}O, and in the continuous mixing approximation we find that the final ^{17}O abundance (after 10 separate mixings) is approximately 5 times larger than the $10^{-3}H_p$ case. The fact that the abundance of this isotope is even more enhanced in the case of continuous mixing is especially interesting in view of the observation of enhanced ^{17}O in IRC 10216. Also the fact that all of the other isotopic abundances obtained in the continuous mixing approximation are within a factor of 3 of the abundances in the one-time mixing of $10^{-3}H_p$ indicates the relative insensitivity of the isotopic abundances to the actual mixing approximation.

c) *Splitting of the Convective Zone*

Sweigart (1974) investigated the response of the intershell convective zone to different amounts of hydrogen mixing in a 0.7 $M_\odot$ Population II star. Using the maximum amount of hydrogen that Schwarzschild and Härm (1967) found to be mixed into the intershell region ($10^{-7}\ M_\odot$, which is approximately equal to our

case of $10^{-3}H_p$), Sweigart did not find any extension of the convective zone into the hydrogen shell. For a mixing rate of 10 times the rate of Schwarzschild and Härm, Sweigart again did not find any extension of the convective zone. He did, however, find evidence that this rate of hydrogen mixing might cause the convective zone to split into two separate convective regions separated by a thin radiative shell. We examined the effects of burning $2.7 \times 10^{-6}\ M_\odot$ (equal to $10^{-2}H_p$) of hydrogen in a thin shell separating the intershell convective region. We arbitrarily located the shell at $T \approx 10^8$ K, and the mass above the shell was approximately $5 \times 10^{-4}\ M_\odot$. After the luminosity due to hydrogen burning dropped to less than $10^3\ L_\odot$ (in a time of 1.7×10^5 s), we then diffused the matter down to the helium shell in the same manner that was used for the diffusion of $10^{-3}H_p$. (We chose a limiting luminosity of $10^3\ L_\odot$, as this should be a lower limit to the luminosity due to the helium shell flash in the outer regions of the convective zone and this is consistent with the helium shell luminosity that Sweigart 1974 found at the outer edge of the convective zone when it was not split.) The results of this shell burning followed by diffusion are shown in Figure 4.

We note that qualitatively the behavior of the isotopes in the case of shell burning followed by the diffusion of $10^{-2}H_p$ is the same as the diffusion of $10^{-3}H_p$ illustrated in Figure 2. Again there is the rapid decline in the hydrogen abundance and the redistribution of the CNO isotopes with a decrease in the ^{12}C abundance while the abundances of ^{13}C, ^{14}N, ^{17}O, and ^{15}N are increasing. We also note the rapid drop in ^{14}N and the buildup of ^{14}C along with a slight hydrogen increase at $T \sim 280 \times 10^6$ K due to the ^{14}N$(n, p)^{14}$C reaction. The neutrons are produced as in the earlier case by the ^{13}C$(\alpha, n)^{16}$O reaction; and some, but not all, of this neutron flux is absorbed by the ^{12}C$(n, \gamma)^{13}$C reaction which contributes to the decrease in ^{12}C at $T > 280 \times 10^6$ K. Quantitatively the isotopic abundances are different for the case of $10^{-2}H_p$ and $10^{-3}H_p$. For example, Figure 4 indicates that the ^{14}C mass fraction in the intershell region becomes larger than ^{13}C$(\sim 10^{-3})$, unlike the case of $10^{-3}H_p$.

As in the case of $10^{-3}H_p$ diffusion, we find an enhancement of ^{17}O in the case of the shell burning of $10^{-2}H_p$. Unlike the former case, in the latter case we find a large enhancement of the mass fraction of ^{18}O in the intershell region; and in parts of the high-temperature regions above the helium shell the ^{18}O abundance is actually larger than the ^{17}O abundance. In this particular mixing approximation, therefore, enhanced ^{18}O can be produced and subsequently mixed outward into the convective envelope.

It was clear from Figure 3 that, although the ^{15}N abundance is initially small in the intershell region, it will increase with time. In the case where we mixed in a substantially larger amount of matter ($10^{-2}H_p$) we found a marked increase in the ^{15}N abundance as shown in Figure 4. At the very high temperatures ($T > 280 \times 10^6$ K) near the helium shell the ^{15}N abundance begins to drop again, primarily due to the ^{15}N$(p, \alpha)^{12}$C reaction.

d) Continuous Mixing of 10^{-2} Pressure Scale Heights

To determine what variations in the isotopic abundances might occur as a result of using the shell-burning approximation we compared the results with the results obtained in the continuous mixing approximation. Figure 5 indicates the results of mixing in $10 \times 10^{-3}H_p$ in the same manner as we mixed in $10 \times 10^{-4}H_p$ shown in Figure 3. We note the same general trends in both the shell burning of $10^{-2}H_p$ followed by diffusion and the continuous mixing and diffusion of $10 \times 10^{-3}H_p$. For instance, in both cases we see gradual depletions of ^{12}C and ^{13}C while ^{16}O, ^{17}O, ^{14}C, ^{18}O, and ^{15}N gradually become enhanced. Quantitatively there are some differences in the final isotopic abundances due to the two different modes of mixing. We note that in both Figures 4 and 5 the ^{13}C mass fraction is decreasing, but in the shell-burning case the ^{13}C abundance is not as depressed as it is in the case of continuous mixing. The repeated injections of matter allow the ^{13}C$(\alpha, n)^{16}$O reaction to deplete the final ^{13}C mass fraction to a value approximately 8 times smaller than the final ^{13}C abundance in the shell-burning case. The concomitant buildup of ^{16}O as shown in Figure 5 is slightly larger ($\sim$2.5 times) than in the shell-burning case. This ^{16}O can then capture protons to form ^{17}F which β^+-decays to ^{17}O. In the case of the shell burning though, by the time ^{16}O has begun to be enhanced ($T \sim 240 \times 10^6$ K) the hydrogen that was initially mixed into the intershell region has been drastically reduced. The hydrogen necessary for the ^{16}O$(p, \gamma)^{17}$O$(\beta^+\nu)$ reaction is being supplied by the ^{14}N$(n, p)^{14}$C reaction. We have a somewhat different case in continuous mixing. Each time hydrogen is mixed into the convective region it is rapidly depleted; but since hydrogen is being periodically injected into the intershell region, there is a new supply of hydrogen available for the enhanced ^{16}O to capture. Thus we find the ^{17}O abundance in the case of continuous mixing to be appreciably larger (a factor of approximately 20) than in the case of shell burning. More observations of ^{17}O in evolved objects like IRC 10216 might help to differentiate between these two mixing models that give appreciably different results for the ^{17}O isotope.

It is also clear from Figures 4 and 5 that the final ^{18}O abundance is quite different for the two different mixing models. The ^{18}O is primarily produced in both cases by the ^{14}N$(\alpha, \gamma)^{18}$F$(\beta^+\nu)^{18}$O reaction, with a lesser contribution from the ^{17}O$(p, \gamma)^{18}$F$(\beta^+\nu)^{18}$O reaction. In case of shell burning followed by diffusion the ^{14}N abundance becomes enhanced and then becomes drastically depleted by burning at $T > 280 \times 10^6$ K. Before the ^{14}N is burned, some of it is converted to ^{18}O. In the case of shell burning of $10^{-2}H_p$, the ^{14}N abundance becomes enhanced to a very large mass fraction ($\sim 10^{-2}$) before becoming depleted. In the continuous mixing case, after the first $10^{-3}H_p$ has been mixed into the intershell region the ^{14}N also becomes enhanced before being rapidly depleted at high temperatures. It is clear from Figure 3, however, that the ^{14}N abundance only reaches a peak mass fraction of approximately 10^{-4}. Furthermore, when the next

$10^{-3}H_p$ is mixed in, the ^{14}N abundance is quite low, as shown in Figure 5, and thus the ^{14}N abundance in the continuous mixing model never approaches very large mass fractions. The net effect is that even though the ^{18}O abundance is increasing with repeated mixing, the final ^{18}O abundance is approximately a factor of 25 less than the final ^{18}O abundance in the shell-burning case. It is significant that we find enhanced ^{18}O only in the case of a single injection of a relatively large amount of matter ($\sim 3 \times 10^{-6}\ M_\odot$) into the intershell convective region. Clearly, observations of enhanced ^{18}O in evolved stars would restrict the number of plausible models for the mixing and nucleosynthesis occurring in red giants.

e) *Production of* ^{14}C

Figures 2–5 clearly indicate a definite enhancement of ^{14}C as a result of matter from the envelope being injected into the intershell region. As we have already pointed out, the ^{14}C results from neutron capture on ^{14}N and the neutrons are produced by the ^{13}C$(\alpha, n)^{16}$O reaction. For our run of temperatures and densities the ^{22}Ne$(\alpha, n)^{25}$Mg reaction does not appreciably contribute to neutron production. Also we found no appreciable buildup of ^{14}C due to static hydrogen shell burning that occurs in evolved stars. Iben (1975) has shown that the hydrogen shell in a 7 $M_\odot$ red giant evolving through the double-shell phase of evolution has a temperature of approximately 85×10^6 K. Using this temperature, a density of 10^2 g cm^{-3}, and an evolutionary time scale of 10^6 years, we found a maximum ^{14}C mass fraction of only 7×10^{-7} in the burning region.

For the case where we mixed in $10^{-2}H_p$ of matter (illustrated in Figs. 4 and 5) the ^{14}C abundance is larger than the ^{13}C abundance by the time matter has mixed into the region just above the helium shell. We assume that for convective mixing these abundances will be found throughout the intershell region. Thus an upper limit to the amount of ^{14}C produced when $10^{-2}H_p$ of matter is injected between the two shells is given by

$$M(^{14}\mathrm{C}) \approx 10^{-3} \times 0.007\ M_\odot = 7 \times 10^{-6}\ M_\odot\ .$$

As we noted previously, the final ^{13}C intershell abundance varies somewhat, depending on the actual mixing approximation. If we assume a rough average ($X_{^{13}\mathrm{C}} \approx 5 \times 10^{-4}$) for the two cases shown in Figures 4 and 5, then the maximum ^{13}C in the intershell region after $10^{-2}H_p$ has been mixed in and burned will be $\sim 3.5 \times 10^{-6}\ M_\odot$, and the mass of ^{12}C will be approximately $7 \times 10^{-4}\ M_\odot$.

Iben (1975) has shown that it is possible for the base of the convective envelope to extend into the intershell region (after the convective zone has disappeared) and convect processed matter out into the envelope. This synthesized matter will obviously then be diluted. In the case of an intermediate mass star of 5–7 $M_\odot$ with a 1 $M_\odot$ core, mass loss may occur in an advanced evolutionary stage. If the star has evolved to the point where the envelope contains 1 $M_\odot$ of roughly solar composition, then the mass of ^{13}C and ^{12}C in that envelope will be $M(^{13}\mathrm{C}) \approx 5.6 \times 10^{-5}\ M_\odot$ and $M(^{12}\mathrm{C}) \approx 4.5 \times 10^{-3}\ M_\odot$, respectively. (Clearly these numbers are approximate since earlier CNO processing in the hydrogen shell might have produced some variations from the solar ^{12}C and ^{13}C values in the envelope.) The ratio of ^{13}C/^{14}C and ^{12}C/^{14}C in the envelope depends on how much of the intershell region is convected outward into the envelope. Stellar model calculations (Iben 1975; Christy-Sackmann 1976) indicate that a substantial fraction of the intershell region ($\sim 30\%$ by mass) is convected into the red giant envelope between helium shell flashes. It follows that the ^{14}C/^{13}C ratio in a red giant envelope of 1 $M_\odot$ should approach an upper limit of ~ 0.1. The ratio of ^{14}C/^{13}C could be even more favorable if the mass of the envelope was smaller than 1 $M_\odot$ when the intershell material was mixed outward. It should also be noted that this process would allow some enrichment of the ^{12}C in the envelope.

Even if substantially smaller fractions of the intershell region ended up in the envelope, ^{14}C might still be observable in very evolved stars. At present an upper limit of $(\mathrm{H}^{14}\mathrm{CN}/\mathrm{H}^{13}\mathrm{CN}) < 1/26$ has been measured in the carbon star IRC 10216 (Kuiper *et al.* 1976). With improvements in the receiver and a larger telescope (assuming the size of the HCN source is not greatly extended) the upper limit of ^{14}C detection using millimeter observations might eventually be $\mathrm{H}^{14}\mathrm{CN}/\mathrm{H}^{13}\mathrm{CN} \lesssim 1/500$ (Zuckerman 1976). Observations to detect ^{14}C in objects like IRC 10216 using millimeter observations and infrared observations of the 2 μm ^{14}C^{16}O bands could provide new insight into how the burning and mixing processes are occurring in red giants.

In making our calculations we have neglected the effects of (n, γ) reactions on heavier elements such as ^{56}Fe. Even though the cross section for the ^{56}Fe$(n, \gamma)^{57}$Fe reaction, as listed by Woosley *et al.* (1975), is approximately 9 times larger than the cross section for the ^{14}N$(n, p)^{14}$C reaction (FCZ II), the ^{14}N abundance is much greater than iron in the matter convected into the intershell region. This follows from our assumption that virtually all of the ^{12}C and ^{16}O above the hydrogen shell are in the form of ^{14}N as a result of CNO processing. Since the nuclear rate equations are governed by the product of the cross sections and the abundances, the relative contribution of the ^{56}Fe$(n, \gamma)^{57}$Fe reaction is less than the relative contribution of ^{14}N$(n, p)^{14}$C. Thus our results are not significantly affected by the neglect of (n, γ) reactions on ^{56}Fe.

We should also note that for a 1 $M_\odot$ core, one might expect the intershell region to have a mass of only $1.8 \times 10^{-3}\ M_\odot$ (Paczynski 1975). This would imply that our intershell mass was a factor of 3.9 times too large. However, significantly larger intershell masses are predicted for even slightly smaller core masses (e.g., 0.9 $M_\odot$). The use of a slightly smaller core mass would have very little effect on our calculated abundances, and would in fact seem to imply luminosities

that are in agreement with recent observations (Feast, Catchpole, and Glass 1976).

Finally we want to emphasize that our calculated ratios of $^{14}C/^{13}C$ are based on dilution in a 1 $M_\odot$ envelope. Stellar evolutionary studies and observations have indicated that evolved stars lose mass and there may be even less mass in the envelope when ^{14}C (and other isotopes) are mixed outward. Thus there may be even less dilution than we have assumed.

f) *The i-Process*

As we mentioned earlier, the large enhancement of ^{14}C in our models results from the $^{14}N(n, p)^{14}C$ reaction and the neutrons are principally produced by the $^{13}C(\alpha, n)^{16}O$ reaction. Once the ^{14}N abundance begins to drop, the neutron flux increases; and even though there are other neutron poisons around [such as $^{13}N(n, p)^{13}C$ and $^{12}C(n, \gamma)^{13}C$], the neutron flux is not completely quenched. We have recorded in detail the neutron abundance as a function of temperature and time. The neutron mass fraction was initially set equal to zero. By the time matter is mixed down to the helium shell ($t = 7.2 \times 10^4$ s), the neutron mass fraction was between 3×10^{-12} and 10^{-10}, depending on how much matter (between 10^{-4} and $10^{-2} H_p$) was mixed into the intershell region. (The maximum neutron mass fraction for the shell burning of $10^{-2} H_p$ was approximately 10^{-10}, although it is not plotted in Fig. 4). The neutron mass fraction is plotted in Figures 3 and 5 for the continuous mixing models. The neutron mass fraction as seen from the graphs varies between 3×10^{-12} and 10^{-10}. The time scale, however, for the continuous mixing cases is 10 times longer (i.e., 7.2×10^5 s) than the diffusion time for the mixing of $10^{-3} H_p$ shown in Figure 2. Since the neutron number density N_n is given by

$$N_n = \rho N_A X_n , \tag{7}$$

where X_n is the neutron mass fraction, and since near the helium shell the density $\rho \approx 1\text{–}2 \times 10^3$ g cm^{-3}, we find

$$N_n \sim 10^{15}\text{–}10^{17} \text{ cm}^{-3} . \tag{8}$$

According to Clayton (1968) the approximate number density of neutrons required for the *s*-process is $N_n \approx 10^5$ cm^{-3}, while for the *r*-process $N_n \approx 10^{23}$ cm^{-3} is required. It is clear that our computed neutron number densities fall between these two values. Recent work by Blake and Schramm (1975) has shown that the neutron flux required for the *s*-process is $F_n \approx 10^{15}$–10^{16} cm^{-2} s^{-1} (or $N_n \approx 2 \times 10^7$ cm^{-3}). If we assume a thermal velocity

$$v_{th} = (2kT/m)^{1/2} \approx 10^8 \text{ cm s}^{-1} , \tag{9}$$

where m is the mass of the neutron and $T \sim 10^8$ K, then our maximum neutron flux is given by

$$F_n = N_n v_{th} \approx 10^{23}\text{–}10^{25} \text{ cm}^{-2} \text{ s}^{-1} . \tag{10}$$

Again this flux is many orders of magnitude larger than what Blake and Schramm (1975) find is required for *s*-process nucleosynthesis. Thus it appears that our values for the neutron flux would allow some form of intermediate neutron process (*i*-process).

The maximum rate of neutron production in our models is roughly 10^{16} cm^{-3} in $\sim 3 \times 10^2$ s or approximately 10^{14} cm^{-3} s^{-1}, and this maximum rate continues over periods of several thousand seconds in the high-temperature regions above the helium shell. Figure 5 indicates, though, that the mass fraction of neutrons in the intershell region remains high over approximately 10^6 s (i.e., 10 diffusion time periods). Although we have not followed the neutron production beyond this time, it is reasonable to assume that neutron synthesis will continue via the $^{13}C(\alpha, n)^{16}O$ reaction in the 10–100 years that the intershell convective zone exists. Since this zone may reappear every 5,000–30,000 years, this neutron production process could provide ample neutrons for nucleosynthesis. Thus we suggest that there may be an intermediate neutron process as well as a slow and rapid process. Perhaps this *i*-process could produce many of the elements identified as *s*-process elements and perhaps some of the elements that are thought to be produced by a combination of *s*- and *r*-processes.

Recently Blake and Schramm (1976) have suggested an alternative neutron process that might produce elements identified as *r*-process elements. They suggest that novae and supernovae would be possible sites for such a process and the conditions required would be less extreme than normally required for the *r*-process. Our calculated neutron number densities are within a factor of several hundred of the number densities that Blake and Schramm (1976) predict to be sufficient to reproduce the calculated abundances of the heavy elements with an A of 160–290. It is conceivable that red giants with somewhat more extreme conditions than the ones we have used might produce neutron number densities that are a factor of several hundred higher than our calculated number densities. If that is the case, perhaps a number of *r*-process elements could be synthesized in certain red giants.

Because the neutron number densities that we have estimated for the *i*-process (10^{15}–10^{17} cm^{-3}) are significantly lower than those chosen by Blake and Schramm (1976), calculations of heavy-element abundances peaks produced by neutrons in the intershell convective zone may lie between the *s*- and *r*-process abundance peaks observed in solar system material. Future calculations may be able to place limits on the amount of such *i*-processed material that can be ejected from stars.

IV. CONCLUSIONS

We have examined several cases where various amounts of hydrogen-rich material are mixed into the intershell convective zone. We conclude the following:

1. Neutron capture on ^{14}N via the $^{14}N(n, p)^{14}C$ reaction will produce relatively large amounts of ^{14}C in the intershell region. When $10^{-2} H_p$ of matter from the hydrogen shell is mixed into the convective zone,

the ^{14}C mass fraction will become 10^{-3}. If substantial portions of this intershell region are mixed out into the 1 $M_\odot$ envelope of a red giant, the ratio of $^{14}C/^{13}C$ should approach 0.1. For a smaller mass envelope the dilution factor will consequently be less and the $^{14}C/^{13}C$ ratio will be larger. Thus ^{14}C may be detectable in evolved stars such as carbon stars by millimeter or infrared observations.

2. An intermediate neutron process (*i*-process) may operate in evolved red giants. We find a neutron number density of $\sim 10^{15}$–10^{17} cm^{-3} and a flux of $\sim 10^{23}$–10^{25} cm^{-2} s^{-1}. The neutrons are principally produced by the $^{13}C(\alpha, n)^{16}O$ reaction.

3. In all cases studied we find substantial enhancements of ^{17}O. These mixing models offer a plausible explanation of the observations of enhanced ^{17}O in IRC 10216.

4. If relatively large amounts of matter ($\geq 10^{-2} H_p$) are rapidly mixed into the intershell region, significant enhancements of ^{18}O and ^{15}N will occur. In some instances ^{18}O will be more abundant than ^{17}O in the intershell convective region. Observations of enhanced ^{18}O or ^{15}N in evolved stars would restrict the number of plausible models for the mixing and nucleosynthesis occurring in red giants.

We would like to thank Dr. B. Zuckerman and Dr. I.-J. Christy-Sackmann for helpful discussions. Computer time for this research was very generously supplied by the University of Maryland Computer Science Center. Partial financial support for this work was provided to one of us (J. J. C.) by NASA grant NGL 21-002-033 to the University of Maryland.

REFERENCES

Blake, J. B., and Schramm, D. N. 1975, *Ap. J.*, **197**, 615.
———. 1976, *Ap. J.*, **209**, 846.
Castellani, V., Giannone, P., and Renzini, A. 1971, *Ap. Space Sci.*, **10**, 340.
Christy-Sackmann, I.-J. 1976, private communication.
Christy-Sackmann, I.-J., and Paczynski, B. 1975, *Mém. Roy. Soc. Liège*, Ser 6, **8**, 335.
Clayton, D. D. 1968, *Principles of Stellar Evolution and Nucleosynthesis* (New York: McGraw-Hill).
Cogan, B. 1975, *Ap. J.*, **201**, 637.
Cowan, J. J., and Rose, W. K. 1975, *Ap. J.* (*Letters*), **201**, L45 (Paper I).
Dearborn, D., and Schramm, D. N. 1974, *Ap. J.* (*Letters*), **194**, L67.
Despain, K. H. 1975, Ph.D. dissertation, California Institute of Technology.
Feast, M. W., Catchpole, R. M., and Glass, I. S. 1976, *M.N.R.A.S.*, **174**, 81P.
Fowler, W. A., Caughlan, G. R., and Zimmerman, B. A. 1967, *Ann. Rev. Astr. Ap.*, **5**, 525 (FCZ I).
———. 1975, *Ann. Rev. Astr. Ap.*, **13**, 69 (FCZ II).
Gingold, R. A. 1974, *Ap. J.*, **193**, 177.
Goldreich, P., and Schubert, G. 1967, *Ap. J.*, **150**, 571.
Iben, I. 1975, *Ap. J.*, **196**, 525.
James, R. A., and Kahn, F. D. 1970, *Astr. Ap.*, **5**, 232.
Kippenhahn, R. 1969, *Astr. Ap.*, **2**, 309.
Kuiper, E. N. R., Kuiper, T. B. H. Zuckerman, B., and Kakar, R. K. 1976, preprint.
Levy, E. H., and Rose, W. K. 1974, *Ap. J.*, **193**, 419.
Maeder, A. 1975, *Astr. Ap.*, **40**, 303.
Paczynski, B. 1975, *Ap. J.*, **202**, 558.
Rank, D. M., Geballe, T. R., and Wolman, E. R. 1974, *Ap. J.* (*Letters*), **187**, L111.
Rolfs, C., and Rodney, W. S. 1974, *Ap. J.* (*Letters*), **194**, L63.
Rood, R. T., and Ulrich, R. K. 1974, *Nature*, **252**, 366.
Rose, W. K. 1968, *Ap. J.*, **152**, 245.
Rose, W. K., and Smith, R. 1970, *Ap. J.*, **159**, 903.
———. 1972, *Ap. J.*, **173**, 385.
Roxburgh, I. W. 1965, *M.N.R.A.S.*, **130**, 223.
Sanders, R. H. 1967, *Ap. J.*, **150**, 971.
Schwarzschild, M., and Härm, R. 1967, *Ap. J.*, **150**, 961.
Shaviv, G., and Salpeter, E. E. 1973, *Ap. J.*, **184**, 191.
Starrfield, S., Truran, J. W., Sparks, W. M., and Kutter, G. S. 1972, *Ap. J.*, **176**, 169.
Sweigart, A. V. 1974, *Ap. J.*, **189**, 289.
Wagoner, R. V. 1969, *Ap. J. Suppl.*, No. 162, **18**, 247.
Woosley, S. E., Fowler, W. A., Holmes, J. A., and Zimmerman, B. A. 1975, preprint.
Zuckerman, B. 1976, private communication.

Note added in proof.—Recent measurements of IRC 10216 by T. G. Barnes, R. Beer, K. H. Hinkle, and D. L. Lambert (preprint 1976) confirm that the ^{17}O abundance is enhanced but indicate an isotopic abundance ratio $^{12}C/^{14}C \gtrsim 10^4$. H. Nørgaard (preprint 1976) has recently pointed out that several important reactions in the study of high-temperature CNO cycle burning involve unstable nuclei whose cross sections have not been measured experimentally. The production of mass 18 nuclei is particularly sensitive to the rates of the reactions $^{18}F(p, \alpha)^{15}O$ and $^{18}F(p, \gamma)^{19}Ne$. It follows that the abundance of ^{18}O need not be enhanced by hot CNO cycle burning as indicated by the calculations of Cowan and Rose (1975). Moreover, the abundances of ^{18}O calculated in this paper may also be too high.

JOHN J. COWAN: Center for Astrophysics, Harvard College Observatory, Cambridge, MA 02138
WILLIAM K. ROSE: Astronomy Program, University of Maryland, College Park, MD 20742